

Characterization of a Pd–Fe bimetallic model catalyst

Marcella P. Felicissimo, Oleg N. Martyanov, Thomas Risse*, Hans-Joachim Freund

Fritz-Haber-Institut der MPG, Department of Chemical Physics, Faradayweg 4-6, 14195 Berlin, Germany

Received 20 October 2006; accepted for publication 14 February 2007

Available online 28 February 2007

Abstract

Small bimetallic Pd–Fe particles supported on a well ordered alumina film grown on NiAl (110) were studied focusing on the geometric, electronic, adsorption, as well as magnetic properties. The morphology, growth mode and surface composition were investigated by combining scanning tunneling microscopy (STM), temperature-programmed desorption (TPD) and infrared spectroscopy (IRAS) using CO as a probe molecule. Information on the electronic properties of the bimetallic systems was obtained by means of X-ray photoelectron spectroscopy (XPS). These measurements were amended by in situ ferromagnetic resonance spectroscopy to address the magnetic properties of the bimetallic particles. The subsequent deposition of the metals at 300 K varying the order of metal deposition resulted in two distinct bimetallic systems. Pd deposited on existing Fe particles forms a shell, however, FMR and XPS suggest that intermixing of Pd and Fe occurs to some extent. For the reverse order, a larger amount of Fe is required to coat Pd particles, due to the strong tendency of Pd to segregate to the surface of the particles.

© 2007 Elsevier B.V. All rights reserved.

Keywords: Model catalyst; Iron; Palladium; Aluminum oxide; XPS; TPD; IRAS; FMR

1. Introduction

The use of a second metallic component has proven to be a suitable method to improve the desired properties of metallic deposits in a variety of different applications such as thin film coating or heterogeneous catalysis. Admixture of a second metallic component has also proven to be an interesting approach to tune the magnetic properties of the systems. For example, the addition of Pt and Pd to ferromagnetic 3d metals, in particular Co and Fe, has gained considerable interest because of large magnetic anisotropy energies (of the order of 0.5 meV per magnetic 3d atom) which makes these systems possible candidates for future magnetic storage device materials [1,2]. In order to tune the catalytic properties of noble metal catalysts bimetallic counterparts were also extensively studied [3,4]. It has been shown that Pd catalysts can be improved towards different

catalytic reactions by the addition of a second metal such as Ag [5], Cu [6], Co [7], Cr [8], Fe [9], or Au [10]. Pd–Fe bimetallic catalysts are mostly used for hydrogenation reactions. Examples for the catalytic activity of this bimetallic system toward the hydrogenation of dienes, nitrobenzene, other aromatic nitro compounds, and CO are described in the literature [9,11,12].

In general the impact of the second metallic component on the properties of the system is usually separated into electronic effects, which are often called ligand effect in this context, and simple geometric considerations concerning the availability of certain sites, known as ensemble effect [13]. However, it is important to bear in mind that these two effects are usually interconnected. While alloying Pd catalysts, which are known to have high selectivity for the production of methanol from synthesis gas [14–16], with small amounts of Fe ($\text{Fe/Pd} < 1$) resulted in an enhancement of the catalyst selectivity [17], a further increase in the Fe content ($\text{Fe/Pd} 4:1$) leads to total loss of selectivity [18]. This fact calls for a microscopic understanding of the problem. Two factors are regarded

* Corresponding author. Tel.: +49 30 84134218.
E-mail address: risse@fhi-berlin.mpg.de (T. Risse).

important for the reactivity and selectivity in CO hydrogenation, namely the chemisorption mode of CO (dissociative *vs* molecular) and the amount and type of surface hydrogen, i.e., weakly or strongly bond to the surface of the catalyst. In this context, the higher selectivity for the formation of oxygenates for Pd–Fe catalysts has been related to the fact that Fe acts as an inert breaker of the Pd ensembles and forms alloy sites for the bridging form of CO chemisorption [18].

In view of the complexity of the processes taking place on such catalysts, metal particles deposited on well ordered oxide supports such as alumina, silica or magnesia under well defined ultrahigh vacuum conditions have been extensively studied as model catalysts [19–21]. Using ultra-thin oxide films grown on a metallic substrate has proven to be a suitable support for metal particles [22]. On the one hand these oxide films resembles a variety of important physical properties characteristic of the bulk material and on the other hand they allow for the application of a large number of established electron based surface science techniques. Metal particles are then prepared by subsequent deposition of metal atoms from the gas phase onto the oxide film and characterized in terms of geometric and electronic structure or adsorption behavior.

The catalytic and magnetic properties, in case of ferromagnetic constituents, of bimetallic particles depend not only on the overall composition and size of the particles, but also on the distribution of the constituents within the clusters. To this end a detailed microscopic understanding of the interaction between Pd and Fe in bimetallic model systems prepared under ultrahigh vacuum conditions is essential. Herein, we present the characterization of Pd–Fe particles supported on a thin alumina film by a variety of surface science techniques. The morphology of these systems was investigated by *scanning tunneling microscopy* (STM) and the distribution of the constituents within the particles with respect to the system composition and order of metal deposition was studied by *X-ray photoemission spectroscopy* (XPS), *temperature-programmed desorption* (TPD) and *infrared reflection absorption spectroscopy* (IRAS), using CO as a probe molecule. For the system obtained by the deposition of various amounts of Pd on Fe particles, in situ FMR measurements were also performed in order to shed light on possible structural changes occurring within the bimetallic particle.

2. Experimental

The experiments were performed in two different UHV systems. The base pressure was never higher than 2×10^{-10} mbar and both UHV systems were equipped with low energy electron diffraction (LEED), a differentially pumped quadrupole mass spectrometer (QMS) and facilities for ion sputtering, gas dosing and metal evaporation. One of the UHV systems was equipped with an STM stage and an XPS spectrometer. The IRAS, TPD and FMR mea-

surements were performed in the other UHV system described in detail elsewhere [23].

The NiAl (110) crystal was cleaned by repeated cycles of Ar⁺ sputtering and annealing to 1270 K. The alumina film was prepared by two cycles of oxidation with 2×10^{-6} mbar O₂ at 550 K followed by annealing to 1130 K for 3 min. The quality of the alumina film was checked by its characteristic LEED pattern showing sharp diffraction spots. Fe and Pd were deposited on the alumina film at 300 K with a deposition rate of 1 Å/min using a commercial electron beam evaporator (Focus Omicron EFM 3T). The deposited amount was calibrated in situ by a quartz microbalance and is reported as the nominal thickness of a hypothetical continuous layer of the metal deposited on the alumina film given in Ångströms (Å). Throughout this paper we will refer to the nominal thickness, as for instance the term 2 Å Pd particles, is an abbreviation for “Pd particles prepared by deposition of 2 Å Pd” and is not intended to characterize the actual size of the particles. The sample was biased to the voltage of the evaporant during metal deposition to avoid acceleration of metal ions onto the surface. For the IRAS and TPD measurements high purity CO was passed through a liquid nitrogen trap for further purification prior to its introduction into the vacuum chamber.

The STM measurements were taken at tip biases of 4–5 V and tunneling currents of ~ 1 nA. All STM images were subjected to plane correction. XPS data were obtained with an Mg K α X-ray source. The binding energies were referenced against the appropriate substrate feature and the detection was normal to the surface. The IRAS spectra were recorded with a Bio-Rad FT spectrometer at 4 cm⁻¹ resolution. For each spectrum one thousand scans were accumulated and background spectra were recorded using the same settings right after metal deposition and cooling to 35 K. For the IRAS experiments the sample was exposed to different CO coverages at 35 K up to saturation coverage. TPD measurements have been performed subsequently by placing the sample less than 1 mm away from the differentially pumped cap of the quadrupole mass spectrometer. The sample was resistively heated with a heating rate of 1.5 K/s as measured by a commercial controller (Schlichting Physikalische Instrumente) using a W/Re (5% and 26% Re) thermocouple spot-welded to the crystal.

3. Results

3.1. STM

The Pd–Fe bimetallic particles were deposited on a thin alumina film grown on the (110) surface of a NiAl alloy single crystal. The structure of this widely used oxide film has been recently determined by Kresse et al. having an overall stoichiometry of Al₁₀O₁₃ [24]. For simplicity the alumina support will be denoted Al₂O₃/NiAl (110) through out this work. The film exhibits a high degree of long range order and an excellent reproducibility of its

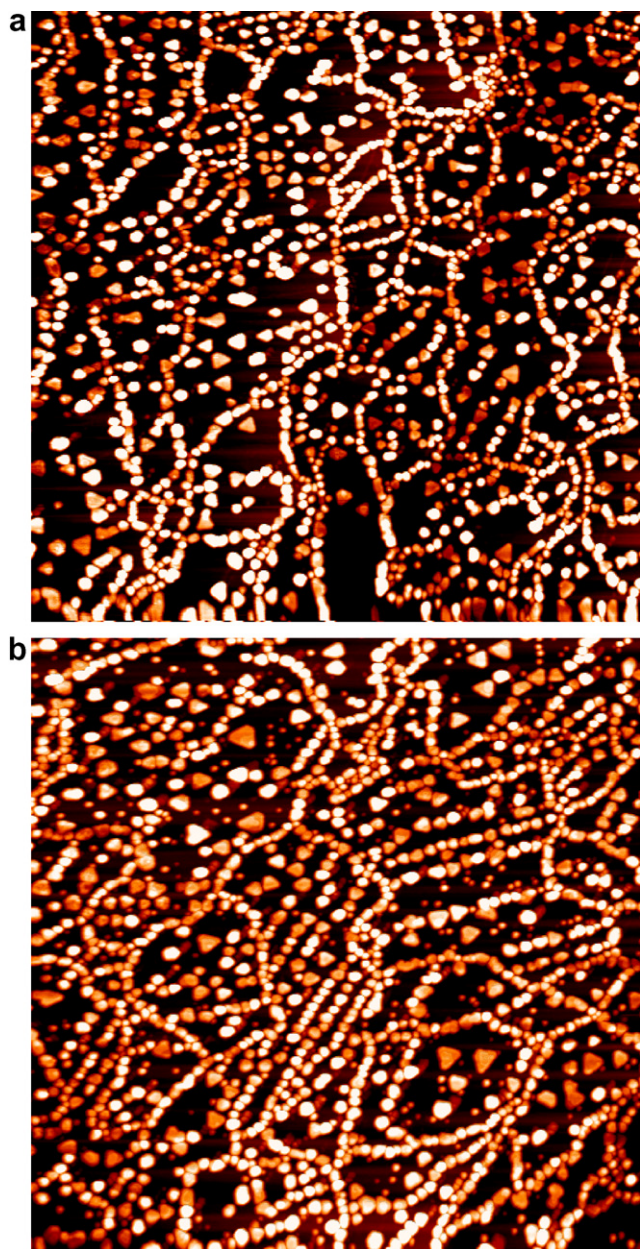


Fig. 1. $300 \times 300 \text{ nm}^2$ STM images of (a) 2 \AA Pd deposited on $\text{Al}_2\text{O}_3/\text{NiAl}$ (110) (4.5 V, 1.0 nA) and (b) subsequent deposition of 2 \AA Fe (3.7 V, 1.2 nA). The depositions were performed at 300 K.

structure, thickness and defect density. In line with previous investigations, Pd deposited at 300 K on the alumina film nucleates at line defects and forms well faceted crystallites with (111) top facets as monitored by STM (Fig. 1a) [25]. The subsequent deposition of 2 \AA Fe on top of 2 \AA Pd particles shows that most of the Fe nucleates on top of Pd particles; however some additional small protrusions are observed which accounts for a 10% increase of the particle density as compared with pure Pd (Fig. 1b). For an analogous Pd–Co system studied in detail by Carlsson et al., a different behavior has been described [26]. In this case, Co nucleates preferentially at point defects of the alumina film and shows a stronger interaction with the oxide

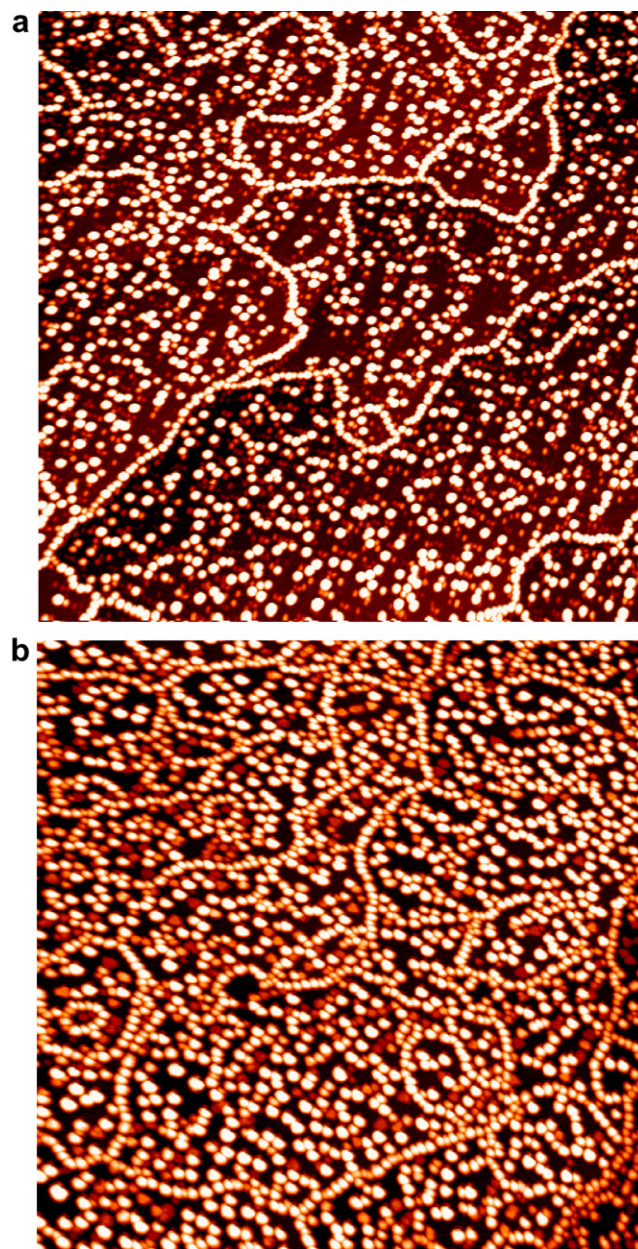


Fig. 2. $300 \times 300 \text{ nm}^2$ STM images of (a) 2 \AA Fe deposited on $\text{Al}_2\text{O}_3/\text{NiAl}$ (110) at 300 K, (4.1 V, 1.3 nA) and (b) subsequent deposition of 2 \AA Pd (4.0 V, 1.7 nA).

surface than Pd, which results in the formation of a larger amount of pure Co particles in between the Pd islands.

On the other hand, if Fe is deposited first a different situation arises. For pure Fe particles deposited at 300 K the STM image (Fig. 2a) shows a bimodal size distribution where larger particles decorate preferentially the line defects and smaller ones nucleate on terraces. For the Fe aggregates no evidence of crystalline order is observed. Upon deposition of Pd on the Fe particles no considerable change in particle density is observed, however, the particle size distribution becomes more homogeneous as seen in Fig. 2b indicating that Pd preferentially nucleates on the small Fe particles.

Thus, the STM results show that independent of the deposition order, bimetallic Pd–Fe particles are formed. However, the STM images do not allow for an examination of the metal distribution within the particles as well as on their surface which is crucial for the understanding of the chemical properties of the system. Therefore, X-ray photoelectron spectroscopy (XPS) as well as infrared reflection absorption spectroscopy (IRAS) and temperature-programmed desorption (TPD) using CO as probe molecule have been performed.

3.2. XPS

Figs. 3 and 4 show the XPS spectra of Pd 3d and Fe 2p levels for various Fe coverages on top of 2 Å Pd. Upon deposition of Fe the Pd 3d level shifts continuously to higher binding energy reaching 0.6 eV after deposition of 4 Å Fe. Concomitantly, the Pd 3d signal intensity decreases. The Fe 2p spectra, on the other hand, show an inverse trend. In this case, a continuous shift to lower binding energy is observed for increasing Fe coverage up to 0.7 eV for 4 Å of Fe. For the opposite order of metal deposition, the XPS spectra of the Pd 3d and Fe 2p level are shown in Figs. 5 and 6. In this case, the deposition of Pd on top of 2 Å Fe particles show a constant binding energy for the Pd 3d core level, independent of Pd coverage. However, the position of this line is shifted by 0.3 eV to higher binding energy with respect to pure Pd particles as observed in Fig. 5. The subsequent depositions of Pd result in a depletion of the Fe 2p signal intensity and a concomitant line broadening. In addition, a continuous shift of the Fe 2p core level towards higher binding energy is observed until a maximum of 0.6 eV after deposition of 4 Å Pd.

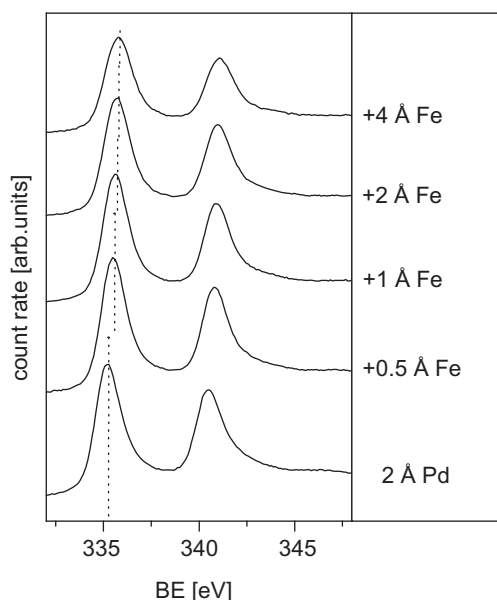


Fig. 3. XPS spectra of Pd 3d level of various amounts of Fe deposited on 2 Å Pd particles.

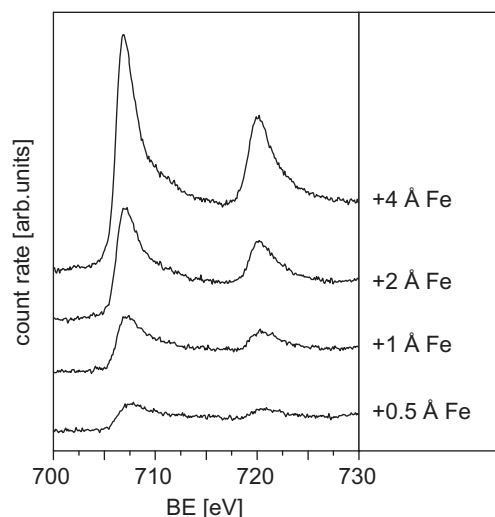


Fig. 4. XPS spectra of Fe 2p level of various amounts of Fe deposited on 2 Å Pd particles.

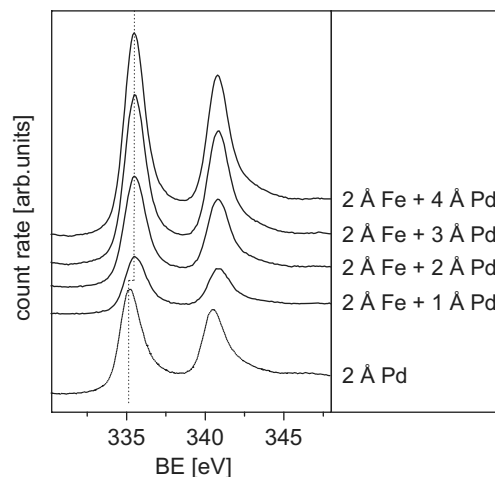


Fig. 5. XPS spectra of Pd 3d level of various amounts of Pd deposited on 2 Å Fe particles. For comparison the XPS spectrum of 2 Å pure Pd particles is shown.

3.3. TPD

The TPD spectra shown in Fig. 7 refer to bimetallic systems obtained by deposition of the indicated amounts of Fe on 2 Å Pd particles at 300 K and subsequent exposure to saturation coverage of CO at 35 K. Each measurement was done on a freshly prepared surface. The bottom most TPD spectrum shown in Fig. 7 refers to the CO desorption from pure Pd particles, which has been described in detail previously and is presented here for comparison with the Pd–Fe bimetallic systems [27]. The next spectrum corresponds to CO desorption from 0.1 Å Fe on top of 2 Å Pd particles resembling the shape of the TPD spectrum of pure Pd particles, however, the position of the high temperature peak, which is assigned to CO desorption from three-fold hollow sites of Pd (111) facets [28], is shifted by about 20 K to lower temperature. Additionally, small

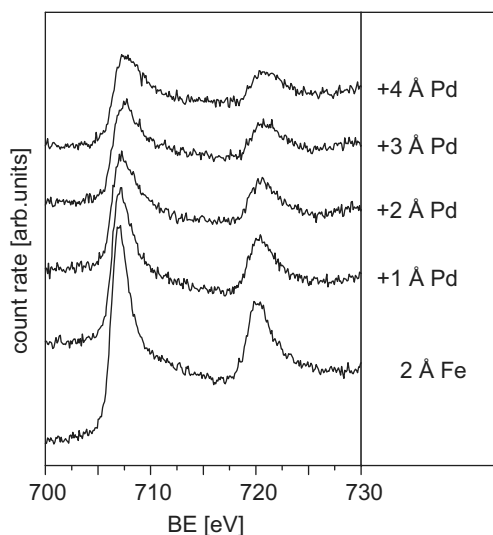


Fig. 6. XPS spectra of Fe 2p level of various amounts of Pd deposited on 2 Å Fe particles.

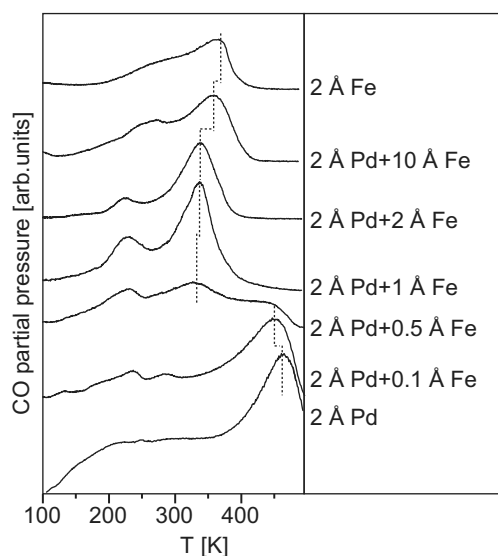


Fig. 7. Temperature-programmed desorption spectra of CO from bimetallic Pd–Fe particles supported on $\text{Al}_2\text{O}_3/\text{NiAl}$ (110). The particles were prepared by depositing 2 Å Pd first and various amounts of Fe subsequently. The spectra for pure Pd and Fe particles are also shown for reference. Prior to TPD the bimetallic surface was exposed to CO saturation coverage at 35 K. The heating rate was 1.5 K/s.

changes are observed in the broad low temperature tail of the spectrum usually attributed to desorption from bridge and on-top sites, which shows two weak extra features also observed for higher Fe coverages. The change of the TPD spectrum becomes more severe already after deposition of 0.5 Å Fe. At this Fe coverage a depletion of the desorption peak of Pd three-fold hollow sites occurs. Concomitantly, a new feature evolves at around 330 K and a low temperature desorption peak at 230 K already seen for 0.1 Å of Fe grows in intensity. Upon the deposition of 1 Å Fe the CO desorption from Pd three-fold hollow sites is no longer

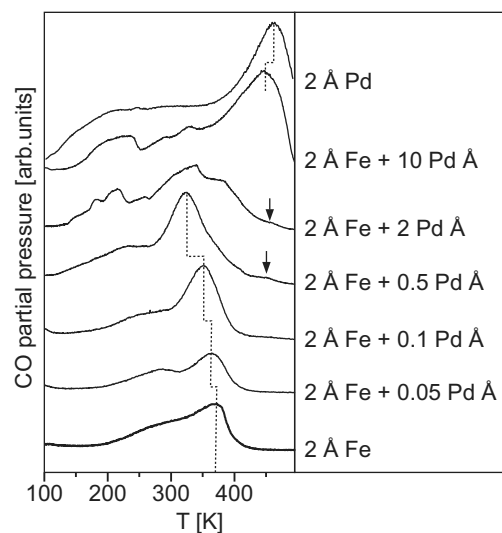


Fig. 8. Temperature-programmed desorption spectra of CO from bimetallic Pd–Fe particles supported on $\text{Al}_2\text{O}_3/\text{NiAl}$ (110). The particles were prepared by depositing 2 Å Fe first and various amounts of Pd subsequently. The spectra for pure Pd and Fe particles are also shown for reference. Prior to TPD the bimetallic surface was exposed to CO saturation coverage at 35 K. The heating rate was 1.5 K/s.

observed and the spectrum is dominated by the feature at 330 K, which shifts to higher desorption temperature with increasing Fe coverage. Finally, after deposition of 10 Å Fe the TPD spectrum approaches the behavior observed for pure Fe particles (top-most spectrum in Fig. 7). Nevertheless, the peak position is still shifted by approximately 10 K to lower temperatures. In addition, the low temperature shoulder observed for pure Fe particles is a more prominent and slightly shifted to lower temperature.

Essentially, two effects can account for the difference in the adsorption and desorption behavior of a bimetallic system in comparison to the pure metals. On the one hand the interaction between adsorbate and the adsorption site may be modified by the presence of the second metal in close proximity, which is usually called a ligand effect. This effect can account for the shift in the desorption temperature. On the other hand, the suppression of the three-fold hollow site can be understood by simple geometric considerations, because high coordination sites such as three-fold hollow sites are more readily depleted by addition of a second metal. This process is often referred to as the ensemble effect. The assignment of peaks observed in the TPD spectra to certain adsorption sites can only be taken as a first indication which is based on comparison with similar bimetallic systems, such as Pd–Co bimetallic particles [29], or data from metal single crystal surfaces.

Pure Fe particles feature two maxima in the TPD spectrum, a high temperature desorption peak at 365 K and a low temperature shoulder with a maximum at 280 K (top-most spectrum in Fig. 7). For Fe single crystal surfaces, the most densely packed Fe (100) surface gives rise to four distinct TPD peaks labeled α_1 (220 K), α_2 (305 K) and α_3 (440 K) at full CO coverage attributed to on-top,

bridge and four-fold hollow sites, respectively, and a peak at 820 K caused by the recombinative desorption of CO from the surface. The four-fold hollow site is believed to be the precursor of the CO dissociation, because the molecule binds to the surface through both atoms (“lying down” configuration) and the C–O bond is therefore strongly weakened [30,31]. The Fe (111) surface, which has a more open structure for the bcc crystal, shows a similar TPD spectrum containing four features at 245 K, 325 K, 400 K and 750 K [32,33]. The “lying down” configuration of CO was also observed for bcc-Fe thin films deposited on Cu (100), however, on fcc-Fe films CO adsorbs only perpendicularly to the surface and no recombinative desorption of CO is observed [34]. For the Fe particles deposited on Al₂O₃/NiAl (110) the limited thermal stability of the system prevents the observation of a recombinative desorption peak. The assignment of the two features observed in the TPD spectrum is not straightforward, because it is difficult to confirm or rule out the presence of the “lying down” CO. In this sense the high temperature desorption peak at 365 K could be attributed to CO desorption from either bridge or four-fold hollow sites and consequently the low temperature desorption peak at 280 K would be related to either bridge or on-top sites. From a simple geometrical model, which implies that about 2 Å Fe are needed to cover completely the Pd particles and based on the TPD behavior of 0.5 Å and 1 Å Fe on top of Pd shown in Fig. 7, it is more likely that the peaks at 365 and 280 K correspond to bridge and on-top sites, respectively.

The subsequent deposition of larger amount of Pd on top of Fe results in a continuous shift of the high temperature peak to lower desorption temperatures. For the deposition of 0.5 and 2 Å Pd on top of Fe a shoulder starts to rise at the desorption temperature of CO from three-fold hollow sites of Pd, which indicates that Pd patches start to form at these metal coverage. Finally, upon the deposition of 10 Å Pd on Fe the spectrum is dominated by the desorption peak of CO from Pd three-fold hollow sites.

3.4. IRAS

Aiming at a better understanding of the adsorption behavior of CO on the Pd–Fe bimetallic systems, IRAS measurements have been performed. Before reporting the obtained results it is of some help to revisit the CO adsorption on pure Pd particles deposited on Al₂O₃/NiAl (110) at 300 K. Small Pd particles (~2 Å nominal thickness) at low CO coverage show IR absorption bands around 1800 and 1900 cm⁻¹, attributed to three-fold hollow and bridge sites respectively, which shift to higher frequencies with increasing CO coverage [35]. At intermediate coverage a band around 1950 cm⁻¹ assigned to bridge-bonded species rises. Finally, at CO saturation coverage the IR-spectrum shows three stretching bands attributed to terminally bonded CO (~2105 cm⁻¹), bridge-bonded species on the terraces of the aggregates (~1953 cm⁻¹) and bridge-bonded species on the

edges of the aggregates (~1988 cm⁻¹). This last feature has been also assigned to CO adsorbed on Pd (100) facets by analogy with the spectrum of Pd single crystal [36]. Pd aggregates grown at room temperature are crystalline and expose mainly (111) and to a smaller extent (100) oriented facets [25]. For these Pd particles the IR stretching band due to bridge-bonded sites on particle edges (1988 cm⁻¹) is more intense than expected on the basis of available sites. In order to explain this observation it has been suggested that the enhancement of the band intensity is due to transfer of intensity via dipole coupling from the band at lower-frequency i.e., bridge-bonded species on the terraces of the aggregates (~1953 cm⁻¹) to that of its high-frequency counterpart [37]. The intensity transfer through dipole coupling is consistent with observations from single crystal surfaces [38].

The deposition of 0.1 Å Fe on top 2 Å Pd has already some impact on the observed IR spectra. At low CO coverage bands assigned to CO adsorbed on Pd three-fold hollow (1818 cm⁻¹) and on Pd (111) bridge sites (1911 cm⁻¹) are observed (Fig. 9). With increasing CO coverage, the band attributed to three-fold hollow sites disappears and the feature assigned to bridge sites shifts to 1958 cm⁻¹. Concomitantly, a band at 1987 cm⁻¹ due to CO adsorbed on Pd (100) bridge sites and particles edges and a band at 2103 cm⁻¹, attributed to Pd on-top sites, appear. Even though the bands stretching frequencies are essentially the same as for the pure Pd case, their relative intensity is changed substantially. For pure Pd particles, at CO saturation coverage the band attributed to bridge sites is more intense than the band of on-top sites while the opposite is observed for the 2 Å Pd + 0.1 Å Fe system.

Fig. 10 shows the IRAS spectra at CO saturation coverage as a function of the amount of Fe deposited on 2 Å Pd particles. The spectra were taken at 35 K and at this temperature it is known that the band at 2163 cm⁻¹ is due to

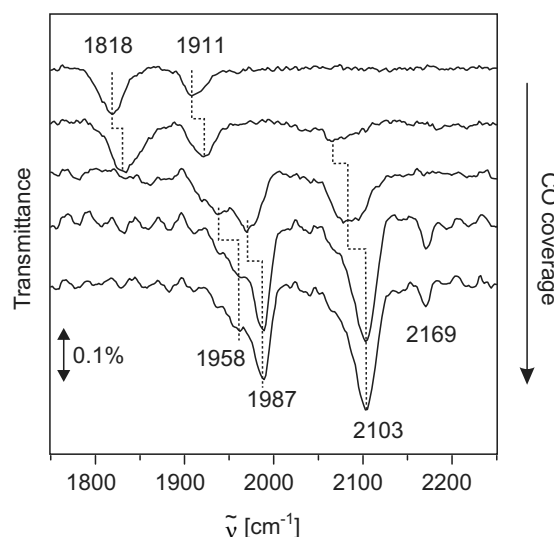


Fig. 9. IR-spectra of adsorbed CO on 0.1 Å Fe deposited on 2 Å Pd particles taken at 35 K as a function of CO coverage.

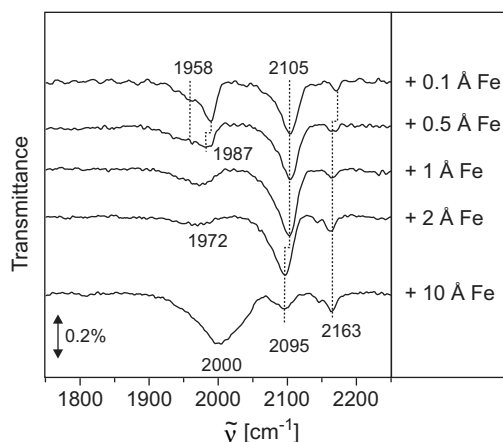


Fig. 10. IR-spectra taken at 35 K for CO saturation coverage on 2 Å Pd particles subsequently covered by various amounts of Fe.

CO adsorbed on the oxide film [39]. After deposition of 0.1 and 0.5 Å Fe the three previously discussed CO stretching bands are observed. With increasing Fe coverage a red shift is observed for Pd on-top sites (2095 cm^{-1}) and the two bands at 1958 and 1987 cm^{-1} are replaced by a band at 1972 cm^{-1} which becomes less intense after addition of 2 Å Fe. After deposition of 10 Å Fe on top of Pd, a broad band at 2000 cm^{-1} appears which is attributed to CO adsorbed on Fe sites [40]. Additionally, the stretching band for Pd on-top sites is still present, indicating that even for large amounts of deposited Fe, Pd still segregates to the surface of the Pd–Fe bimetallic particles. A similar behavior has also been observed for Pd–Co bimetallic particles [41].

In order to correlate the IR and TPD spectra, IRAS measurements of 2 Å Fe deposited on 2 Å Pd particles exposed at low temperature to CO saturation coverage were performed after consecutive flashes of the sample to higher temperatures (Fig. 11). The IR band at 2098 cm^{-1} attrib-

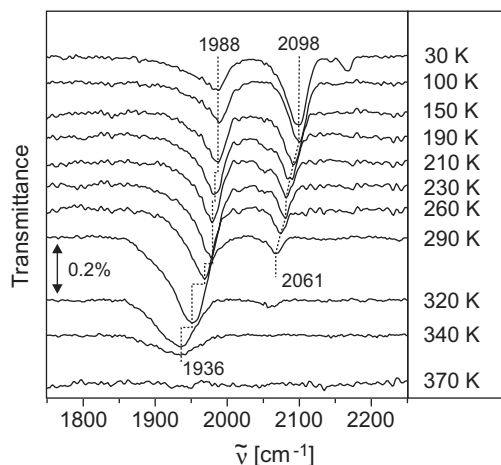


Fig. 11. IR-spectra of CO saturation coverage on 2 Å Fe deposited on 2 Å Pd particles taken at 35 K after annealing to the indicated temperatures.

uted to Pd on-top sites is partially depleted upon heating the system to 260 K, while the peak around 1980 cm^{-1} gains intensity. This indicates that the desorption peak at 230 K is mainly due to desorption of on-top bound CO, even though this state is not fully depopulated as indicated by the IR band observed at 2061 cm^{-1} . This may point to the fact that the peak around 2100 cm^{-1} consists of more than one species with different desorption temperatures which would be in line with observations for the reversed deposition order. Increasing annealing temperatures lead to the occupation of the energetically more favorable bridge sites. After heating the sample to 370 K the feature attributed to bridge sites (stretching frequency at 1936 cm^{-1}) is no longer observed, which would correlate to the most intense TPD signal with a maximum at 335 K.

The IR spectrum of 2 Å Fe particles at CO saturation coverage presents a stretching band at 2030 cm^{-1} attributed to CO adsorbed on Fe on-top sites (Fig. 12) [42]. A rather unexpected result was obtained when 0.1 Å of Pd was subsequently deposited on top of the Fe particles. In this case, already at low CO coverage an intense peak at 2051 cm^{-1} is observed which could be correlated to CO bound on top of somewhat modified Pd sites (data not shown). At full CO coverage the IR spectrum (Fig. 12) is dominated by a band at 2096 cm^{-1} attributed to Pd on-top sites in close contact with Fe atoms. As the amount of Pd deposited on 2 Å Fe is raised to 0.5 Å, the typical bands for CO on-top and bridge sites on Pd are observed, suggesting that the Pd atoms are forming small islands on the Fe particles already at this low Pd coverage. Upon increasing the Pd amount (2 Å) no qualitative change on the IR spectra is observed. At high Pd coverage (10 Å) the IR spectrum resembles the spectrum of pure Pd particles where the band attributed to on-top sites is less intense than the band assigned to bridge sites. This observation corroborates the TPD result, which shows a behavior similar to that of pure Pd for this high amount of Pd deposited on Fe particles.

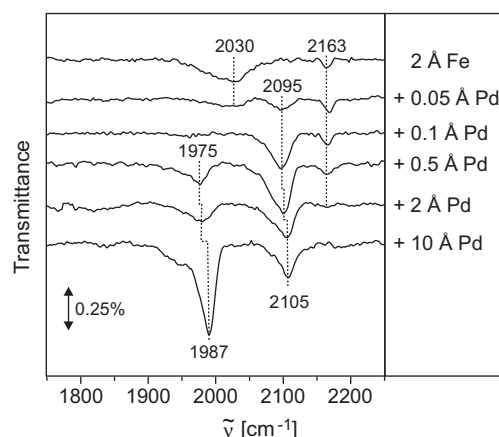


Fig. 12. IR-spectra of adsorbed CO on 2 Å Fe particles after the deposition of various amounts of Pd taken at 35 K.

3.5. FMR

Fig. 13 shows the FMR spectrum of 3 Å Fe deposited on the alumina film at room temperature with the magnetic field being oriented parallel to the surface. The spectrum shows a single rather symmetric peak located at 304 mT. Angular dependent measurements reveal a uniaxial out of plane anisotropy with an easy axis of magnetization parallel to the surface. The difference between the resonance position parallel and perpendicular to the surface is 138 mT (Table 1). Upon subsequent depositions of 1 Å Pd, the apparent resonance position shifts to lower field and the apparent line width increases from 127 to 141 mT. In addition, a second peak starts to evolve at about 300 mT which grows further upon addition of Pd. This results in an increase of the asymmetry of the line shape which is rather pronounced after addition of 5 Å Pd. A similar trend is observed for smaller particles prepared by deposition of 2 Å Fe, however, the two peaks shift to higher fields and their separation diminishes. The shift of the lines to higher fields and the change of their separation are due to increased superparamagnetic fluctuations of the magnetization for particles of smaller size.

From a qualitative inspection of the FMR spectra shown in Fig. 13 it is obvious that the integral intensity of the FMR signal increases with increasing amount of Pd. The intensity of the FMR with respect to the Pd coverage obtained by a proper double integration of the derivative spectra is plotted in the inset of Fig. 13 for 1, 2 and 3 Å Fe particles. It is seen that the FMR intensity for 2 and 3 Å Fe increases up to 5 Å Pd and levels off for higher Pd coverage. It is interesting to note that the relative gain (a factor of 2.5) in the

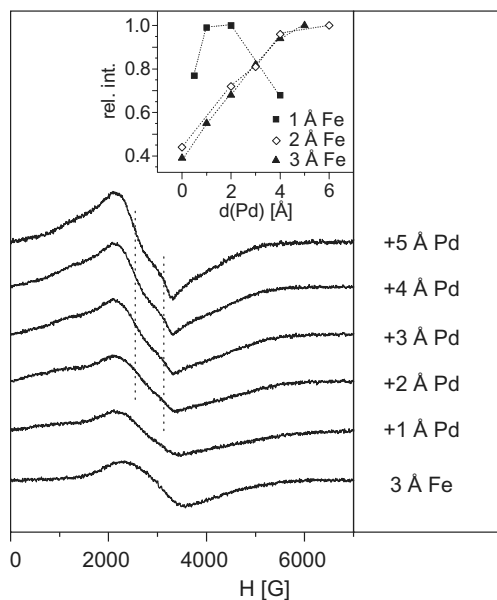


Fig. 13. FMR spectra of 3 Å Fe deposited at room temperature on alumina with increasing Pd coverage. The static magnetic field was oriented parallel to the surface of the crystal. The inset shows the integral intensity of the FMR spectra with respect to the nominal deposition of Pd on top of 1, 2 and 3 Å Fe particles.

Table 1

Apparent resonance positions, line width and difference of resonance position measured in parallel and perpendicular orientation with respect to the surface for Fe particles with subsequent deposition of various Pd amounts

Particles composition	$H_{\text{res}} (90^\circ)$, mT	ΔH_{res} , mT	Line $\Delta H_{\text{p-p}} (90^\circ)$, mT
1 Å Fe	323	15	40
+0.5 Å Pd	318	25	50
+1 Å Pd	322	31	55
+2 Å Pd	322	22	37
+4 Å Pd	322	18	29
2 Å Fe	325	41	96
+2 Å Pd	316	35	71
+3 Å Fe	317	43	69
+4 Å Fe	317	47	63
+6 Å Pd	315	58	51
3 Å Fe	304	138	127
+1 Å Pd	282	146	141
+2 Å Pd	279	153	136
+3 Å Pd	273	167	127
+4 Å Pd	270	178	123
+5 Å Pd	270	188	117

FMR signal intensity is almost the same for both 2 and 3 Å Fe. In contrast to that 1 Å Fe particles show an increase of the FMR signal intensity only for small amounts of Pd (0.5 and 1 Å). The deposition of 2 Å Pd is almost identical to the situation of 1 Å Pd whereas addition of 4 Å Pd leads to substantial reduction of the FMR signal intensity. Interestingly, the reduction of the integral intensity goes along with a decrease of the line width and spectral anisotropy while the initial increase was associated with an increase of line width and spectral anisotropy (Table 1).

4. Discussion

4.1. Pd particles with Fe on top

The STM results have shown that subsequently deposited Fe nucleates mainly on top of Pd particles and based on XPS, IRAS and TPD measurements it was possible to access information about the distribution of the metals within the particles. Based on the fact that Pd has a strong tendency to segregate to the surface in Pd–Fe alloys [43], it is expected that for this system the two metals would have a good chance to intermix. Indeed, the XPS results show that increasing amounts Fe induces significant electronic perturbations on Pd. A similar behavior has been found for $\text{Fe}_{1-x}\text{Pd}_x$ alloys where a strong dependence of the core level shift on the composition is observed. In line with the present result, it has been shown that consecutive higher Fe concentration induces a shift of the Fe 2p to lower binding energy and conversely a shift of the Pd 3d to higher binding energy [44]. Some caution must be taken in the interpretation of core level binding energy shifts, since they may contain contributions of initial state effects, e.g. charge transfer or orbital rehybridization and final state effects, which regard changes in the screening of the core hole.

To some extent the electronic perturbation induced by Fe depositions on top of Pd particles can be interpreted on the bases of charge transfer from Pd to Fe, however, the Pd(4d) \rightarrow Pd(5s,5p) orbital rehybridization may also contribute. It has been extensively shown in the literature that the later effect can account for the binding energy shift observed for Pd in a series of bimetallic systems [45,46]. The continuous shift of the Pd 3d core level with the deposition of increasing quantities of Fe, even above the amount expected to result in the completion of a shell, can be taken as an indication that a simple core shell model is inappropriate to explain the experimental results which also implies that metal intermixing occurs. This assumption is further supported by the TPD and IRAS results. This is evidenced by the presence of the IR band assigned to Pd intermixed sites (2095 cm^{-1}) even at high amount of Fe deposition (10 \AA). Correspondingly, the TPD spectrum taken after deposition of 10 \AA still shows a shift of the main desorption peak and some additional structure at lower temperature (Fig. 7).

The IRAS results show that the deposition of 0.1 \AA Fe, which corresponds to a coverage of about 10% of the Pd particles surface, leads to an increase of the on-top species at the expense of the bridge bound species at CO saturation coverage. This can be understood by means of an ensemble effect which can explain the depletion of three-fold hollow sites after addition of 0.5 \AA Fe. A similar behavior has been observed for an analogous system, Pd–Co, studied in detail previously [29]. In addition to the ensemble effect, the shift of the stretching frequencies to 1988 cm^{-1} (assigned to Pd bridge) and 2098 cm^{-1} (close to the Pd on-top sites) indicate that electronic effects are also present (Fig. 10). It is interesting to notice that the shift of the stretching frequency for on-top bound CO induced by Fe is significantly larger than the corresponding shift for the system Pd–Co [41], while the impact on the desorption temperature is in perfect accord with what has been observed for CO on Pd–Co systems [26].

It is interesting to note that between 1 \AA and 2 \AA Fe deposited on Pd particles the TPD and IRAS spectra show no significant change. Therefore it is inferred that the composition of the top most layers remain relatively stable, despite the fact that the nominal amount of Fe is doubled. This implies that strong intermixing of the metals occurs. Interestingly, there is no direct evidence for bands indicating the presence of Fe bound CO except for the largest metal coverage, even though the presence of Fe can be inferred, e.g. from the shift of the line at around 2100 cm^{-1} . Even at the highest coverage of 10 \AA a significant shift of the CO stretching frequency with respect to the pure Fe particles is observed. First, one has to notice that the IR band of CO on pure Fe particles is rather broad indicating that the CO stretching frequency depends strongly on the local environment. Thus, it is possible that some of the bands, which are assigned to Pd related states due to their proximity to lines observed for pure Pd particles, have contributions from Fe sites influenced by the presence of Pd (see discussion of the reversed deposition order). The general picture inferred from these measurements namely the strong intermixing of the two metals and the presence of Pd at the particles surface even at large Fe coverage is schematically depicted in Fig. 14.

4.2. Fe particles with Pd on top

After deposition of Pd on top of Fe clusters, no additional particles are observed indicating that Pd does nucleate on the Fe particles, however, the bimodal size distribution of the Fe particles become more homogeneous after Pd deposition (see Fig. 2). The effect can be understood by the initial growth of the Fe particles. As seen in Fig. 2a, small particles grow in the vicinity of larger particles that nucleate on the line defects. This results in a partial decoration of the larger particles by the smaller ones, which makes it more likely that a Pd atom impinging on the areas in between the line defects (which is the largest

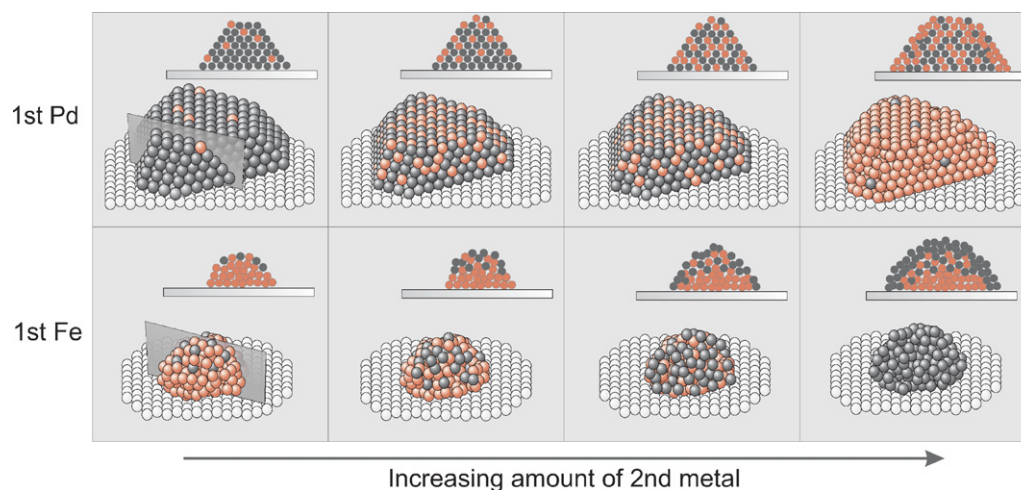


Fig. 14. Schematic representation of the Pd–Fe particles growth mode as inferred based on the STM, XPS, IRAS and TPD measurements.

fraction of surface area) nucleate on the smaller Fe particles that act as a barrier to Pd diffusion.

Based on results from the literature it is expected that Pd should form a shell on top of an Fe core [47]. Nevertheless, the present data shows that some degree of metal intermixing is present when Pd is deposited on Fe particles. The continuous Fe 2p level shift to higher binding energy with increasing amount of Pd deposition and the constant but shifted position of the Pd 3d level in relation to pure Pd are consistent with a constant electronic perturbation for both metals up to a coverage of 4 Å Pd. For a core shell model at low Pd coverage a shift of the Pd 3d level binding energy with respect to the value obtained for pure Pd clusters is expected. However, at higher coverages the binding energy relaxes towards the value observed for pure Pd particles. This is exactly what has been observed for a similar bimetallic system that consists of different Pd coverages on Co particles [26]. In contrast, the binding energy of the Co 2p level for this system does not show any change upon the various Pd depositions.

The influence of Fe on the surface properties of the bimetallic system is further observed in the TPD spectra which documents the influence of Fe on the CO binding energy for Pd coverage up to 2 Å. On the other hand, the IRAS results suggest that higher coordinated adsorption sites with predominant Pd character exist. Already 0.1 Å Pd (less than 10% average surface coverage) changes the IR spectrum completely. The band attributed to pure Fe sites (2030 cm^{-1}) is depleted and no longer visible at the expense of a band at 2095 cm^{-1} while the amount of bound CO as estimated from TPD remains almost constant. It is tempting to assign this IR band to Pd on-top sites modified by the proximity of Fe atoms (Fig. 12). However, for the given surface coverage a simple occupation of Pd sites is not sufficient to explain the TPD results. In addition, the line at 2030 cm^{-1} was assigned to CO bound on top Fe based on comparison with single crystal data. Thus, it is concluded that the band at 2095 cm^{-1} has some contribution of Fe sites influenced by the presence of Pd.

This is further corroborated by the IR spectrum of 0.5 Å Pd deposited on Fe particles at lower CO coverage showing two close stretching bands that merge into a broader band at about 2100 cm^{-1} at CO full coverage. Annealing experiments show the depletion of one feature at about 210 K, which is in good agreement with the CO desorption from Pd on top sites, while the second feature is extinguished after heating to 325 K (data not shown).

A closer inspection of the TPD spectrum of 0.5 Å Pd reveals that in addition to the main peak shifted to lower temperature due to ligand effects [48] a small shoulder appears at a temperature assigned to CO bound to three-fold hollow sites on pure Pd particles (see arrow in Fig. 8). This points to the formation of small Pd patches which is further corroborated by an IR band at 1828 cm^{-1} observed at low CO coverage (data not shown). Along this line, the band at 1975 cm^{-1} observed at CO full coverage is tentatively attributed to Pd bridge sites and is consistent with

the formation of higher coordinated Pd sites on this system.

Despite the observed intermixing of the metals the tendency of Pd to segregate to the surface is well recognizable. To this end it is interesting to note that the IR as well as the TPD spectrum of 0.5 Å Pd on 2 Å Fe particles are similar to those observed for 1 Å Fe deposited on top of 2 Å Pd (Fig. 10). Consequently, the addition of more Pd to Fe clusters changes the surface properties monotonously towards the properties of Pd particles. After the deposition of 2 Å Pd the IR stretching band assigned to Pd on-top sites appears at 2105 cm^{-1} , indicating that Pd is in a Pd rich environment. This observation is in line with the presence of bridge-bonded CO on Pd already pointed out, that indicates the growth of Pd patches on the Fe particles. At the same time the TPD spectrum shows significant alterations of the binding energies as compared to pure Pd particles. Nevertheless, upon deposition of 10 Å Pd the IR as well as the TPD spectra resembles the features observed for pure Pd particles showing that, as expected, at this coverage a Pd shell on top of the Fe particles has been formed.

From these results it can be concluded that Pd forms a shell on top of Fe, however, significant intermixture of the metals occur for smaller Pd coverage, which is in contrast to what has been observed for the Pd–Co system where no indications for intermixing were found based on these methods.

Additional information on the intermixing of metals can be obtained from the FMR measurements due to the influence of the magnetic properties caused by rearrangements taking place in small bimetallic particles [49,50]. The first aspect to mention at this point is the observation of two components within the FMR line that results from the addition of Pd to the pristine Fe particles, which is mainly due to a reduction of the line width rather than large changes of the resonance positions that in this case accounts only for small effect. This observation can be related with the bimodal size distribution observed in the STM image of 2 Å Fe deposited on the alumina film (Fig. 2a). Therefore, the addition of increasing Pd amounts on top of 3 Å Fe particles at room temperature leads to a decrease in line width, which makes evident the presence of at least two lines.

More important for the forthcoming discussion is the behavior of the intensity with increasing Pd coverage indicating a substantial change of the magnetization of the particles upon the addition of Pd. It is worth mentioning that this increase of intensity is not due to an increase of anisotropy or a shift of the Curie temperature as checked by additional experiments not shown here. Several factors can contribute to the enhancement of the magnetic moment. For instance, contributions from induced magnetization of Pd could play a role. It has been shown that metallic Pd is near the threshold of becoming ferromagnetic and it may exhibit an induced magnetic moment when a ferromagnetic impurity is present [51,52]. However, the polarization of Pd alone cannot account for the observed effect

in the view of the fact that the induced magnetic moment per Pd atom is only of the order of a few tenth of μ_B . It is also known that the Fe magnetic moment at the Pd/Fe interface is enhanced, although this would still be a small effect to account for the observed increase of the particle magnetic moment [53]. Therefore, the increase of FMR intensity is likely to be related with an increase of the particle magnetic moment induced by structural rearrangements within the particles, which can lift some of the strain imposed by the nucleation on the alumina surface. This interpretation is in line with the proposed picture, based on the results of other techniques, discussed above.

For the smaller Fe particles (nominal thickness of 1 Å) the FMR signal shows, at first, an increase in intensity and subsequent decrease after the deposition of 4 Å Pd. This behavior can be explained by the same picture described for the larger Fe particles, namely the presence of Pd induces structural rearrangements within the Fe particles. However, for smaller particles the influence of the substrate on the structure of the film is more severe which may allow for an enhanced intermixing of Fe and Pd. In case of a stronger intermixing the particles may behave like Pd–Fe alloys where a decrease of the magnetization is expected [54].

5. Conclusion

The geometric, electronic and adsorption properties of Pd–Fe particles supported on a thin alumina film were studied by means of a variety of surface science techniques. The obtained data indicate that the properties of the bimetallic systems can be tuned by the preparation procedure, namely the order of metal deposition. Based on STM images it has been verified that Fe nucleates mainly on the Pd particles and to less extent between them. If Fe is deposited first a bimodal size distribution is observed and Pd seems to nucleate preferentially on top of the smaller Fe particles. The bimodality of the size distribution could also be verified using FMR.

The detailed characterization of the Pd–Fe systems enables the proposition of a model for the bimetallic particle growth as a function of the order of metal deposition, which is schematically presented in Fig. 14. This schematic representation does not imply that the problem can be reduced to geometric effects only, even though a simple geometric model is shown. The sequential deposition of Fe on top of Pd results in intermixing of the metals. This behavior is likely to be related to the tendency of Pd to segregate to the surface of the particles. For the reversed deposition order Pd finally forms a shell on top of Fe particles, however, a significant amount of intermixing occurs during the initial coverage of the Fe particles. The enhanced tendency of Pd to be at the surface results in rather similar surface properties for particles prepared by deposition of 0.5 Å Pd on top of 2 Å Fe particles and particles obtained by the deposition of 1 Å Fe on top of 2 Å Pd. For these two systems although the surface composition has proven to

be similar the bulk composition is different. Presently, the catalytic properties of these bimetallic systems are studied to acquire information on their catalytic performance towards hydrogenation reactions.

References

- [1] D. Weller, A. Moser, *IEEE Trans. Magn.* 35 (6) (1999) 4423.
- [2] G.H.O. Daalderop, P.J. Kelly, M.F.H. Schuurmans, *Phys. Rev. B* 44 (1991) 12054.
- [3] B. Coq, F. Figueras, *J. Mol. Cat. A* 173 (2001) 117.
- [4] L. Guzzi, *Catal. Lett.* 7 (1990) 205.
- [5] E.A. Sales, B. Benhamida, V. Caizergues, J.P. Lagier, F. Fievet, F. Bozon-Verduraz, *Appl. Catal. A* 172 (1998) 273.
- [6] L. Guzzi, Z. Schay, G. Stefler, L.F. Liotta, G. Deganello, A.M. Venezia, *J. Catal.* 182 (1999) 456.
- [7] A. Sárkány, Z. Zsoldos, Gy. Stefler, J.W. Hightower, L. Guzzi, *J. Mol. Catal.* 157 (1995) 179.
- [8] A. Borgna, B. Moraweck, J. Massardier, A. Renouprez, *J. Catal.* 128 (1991) 99.
- [9] R. Bachir, P. Marecot, B. Didillon, J. Barbier, *J. Appl. Catal. A: Gen.* 164 (1997) 313.
- [10] G.C. Bond, A.F. Rawle, *J. Mol. Catal. A* 109 (1996) 261.
- [11] A.M. Strätz, in: J.R. Kosak (Ed.), *Catalysis of Organic Reactions*, CRC, New York, 1984, p. 335.
- [12] A. Benedetti, G. Fagherazzi, F. Pinna, G. Rampazzo, M. Selva, G. Strukul, *Catal. Lett.* 10 (1991) 215.
- [13] P. Liu, J.K. Nørskov, *Phys. Chem. Chem. Phys.* 3 (2001) 3814.
- [14] W.-J. Shen, M. Okumura, Y. Matsumura, M. Haruta, *Appl. Catal. A* 213 (2001) 225.
- [15] C.-T. Au, T.-J. Zhou, W.-J. Lai, *Catal. Lett.* 62 (1999) 147.
- [16] E. Shustorovich, A. Bell, *Surf. Sci.* 253 (1991) 386.
- [17] L. Guzzi, *Stud. Surf. Sci. Catal.* 38 (1988) 85.
- [18] M. Ichikawa, *Polyhedron* 7 (1988) 2351.
- [19] C.R. Henry, *Prog. Surf. Sci.* 80 (2005) 92.
- [20] M. Bäumer, H.-J. Freund, *Prog. Surf. Sci.* 61 (1999) 127.
- [21] D.W. Goodman, *J. Catal.* 216 (2003) 213.
- [22] C. Xu, D.W. Goodman, in: G. Ertl, H. Knötzinger, J. Weitkamp (Eds.), *Handbook of Heterogeneous Catalysis*, vol. 2, Weinheim, 1997, p. 826.
- [23] J. Schmidt, T. Risse, H. Hamann, H.-J. Freund, *J. Chem. Phys.* 116 (2002) 10861.
- [24] G. Kresse, M. Schmid, E. Napetschnig, M. Shishkin, L. Köhler, P. Varga, *Science* 308 (2005) 1440.
- [25] K.H. Hansen, T. Worren, S. Stempel, E. Lægsgaard, M. Bäumer, H.-J. Freund, F. Besenbacher, I. Stensgaard, *Phys. Rev. Lett.* 83 (20) (1999) 4120.
- [26] A.F. Carlsson, M. Naschitzki, M. Bäumer, H.-J. Freund, *J. Phys. Chem. B* 107 (2003) 778.
- [27] M. Bäumer, J. Libuda, A. Sandell, H.-J. Freund, G. Graw, Th. Bertram, H. Neddermeyer, *Ber. Bunsenges. Phys. Chem.* 99 (1995) 1381.
- [28] H.-J. Freund, *Angew. Chem. Int. Ed. Engl.* 36 (1997) 452.
- [29] M. Heemeier, A.F. Carlsson, M. Naschitzki, M. Schmal, M. Bäumer, H.-J. Freund, *Angew. Chem. Int. Ed.* 41 (2002) 4073.
- [30] D.W. Moon, S.L. Bernasek, J.-P. Lu, J.L. Gland, D.J. Dwyer, *Surf. Sci.* 184 (1987) 90.
- [31] S.D. Cameron, D.J. Dwyer, *Langmuir* 4 (1988) 282.
- [32] U. Seip, M.-C. Tsai, K. Christmann, J. Küppers, G. Ertl, *Surf. Sci.* 139 (1984) 29.
- [33] C.E. Bartosch, L.J. Whitman, W. Ho, *J. Chem. Phys.* 85 (2) (1986) 1052.
- [34] J. Radnik, E. Chopovskaya, M. Grüne, K. Wandelt, *Surf. Sci.* 352–354 (1996) 268.
- [35] K. Wolter, O. Seiferth, H. Kuhlenbeck, M. Bäumer, H.-J. Freund, *Surf. Sci.* 399 (1998) 190.
- [36] D.R. Reiner, M.-C. Wu, D.I. Mahon, D.W. Goodman, *J. Vac. Sci. Technol. A* 14 (1996) 1184.

- [37] K. Wolter, O. Seiferth, J. Libuda, H. Kuhlenbeck, M. Bäumer, H.-J. Freund, *Surf. Sci.* 402–404 (1998) 428.
- [38] P. Hollins, *Surf. Sci. Rep.* 16 (1992) 53.
- [39] R.M. Jaeger, J. Libuda, M. Bäumer, K. Homann, H. Kuhlenbeck, H.-J. Freund, *J. Electron. Spectrosc. Relat. Phenom.* 64/65 (1993) 217.
- [40] T. Wadayama, K. Kubo, T. Yamashita, T. Tanabe, A. Hatta, *J. Phys. Chem. B* 107 (2003) 3768.
- [41] A.F. Carlsson, M. Bäumer, T. Risse, H.-J. Freund, *J. Chem. Phys.* 119 (2003) 10885.
- [42] C. Benndorf, B. Kruger, F. Thieme, *Surf. Sci.* 163 (1985) L675.
- [43] J.C. Bertolini, J.L. Rousset, P. Miegge, J. Massardier, B. Tardy, *Surf. Sci.* 287/288 (1993) 346.
- [44] S.L. Zhang, J.R. Zhang, *Phys. Stat. Sol. B* 182 (1994) 421.
- [45] J.A. Rodriguez, R.A. Campbell, D.W. Goodman, *Surf. Sci.* 307–309 (1994) 377.
- [46] J.A. Rodriguez, in: D.P. Woodruff (Ed.), *Surface Alloys and Alloy Surfaces*, Elsevier, Amsterdam, 2002, p. 439.
- [47] A.V. Ruban, H.L. Skriver, J.K. Nørskov, *Phys. Rev. B.* 59 (1999) 15990.
- [48] J.A. Rodriguez, *Surf. Sci. Rep.* 24 (1996) 223.
- [49] D. Sander, *Rep. Prog. Phys.* 62 (5) (1999) 809.
- [50] T. Risse, M. Mozaffari-Afshar, H. Hamann, H.-J. Freund, *Angew. Chem. Int. Ed.* 43 (2004) 517.
- [51] U. Grandmann, R. Berholz, *Phys. Rev. Lett.* 52 (9) (1984) 771.
- [52] F. Pan, T. Zang, J. Zhang, B.X. Liu, *J. Phys. Condens. Matter* 5 (1993) L507.
- [53] L. Cheng, Z. Altounian, D.H. Ryan, J.O. Strom-Olsen, M. Sutton, Z. Tun, *Phys. Rev. B* 69 (2004) 14.
- [54] J.J.M. Franse, R. Gersdorf, in: *Landolt-Börnstein – Numerical Data and Functional Relationships on Science and Technology*, vol. 19, K.-H. Hellwege, O. Madelung (Eds.), Germany, 1986, p. 596.